JOURNAL OF MATERIALS SCIENCE 32, 3783–3800

Dielectric relaxations in liquid-impregnated porous solids

B. NETTELBLAD
Physics Department, Chalmers University of Technology, S-412 96 Göteborg, Sweden
G. A. NIKLASSON
Teknikum, Uppsala University, Box 534, S-751 21 Uppsala, Sweden

We have studied dielectric relaxation in liquid-impregnated porous solids. The samples were constructed from either glued sand grains or sintered polypropylene beads. We experimentally obtain two relaxations originating from the bulk of the sample. Electrode effects are seen at low frequencies, only for high liquid conductivities. The two bulk relaxations are interpreted as being due to diffusion in the electrochemical double layer surrounding the solid grains, and as a Maxwell–Wagner relaxation due to the heterogeneity of the samples, respectively. The experimental results can be qualitatively reproduced by calculations using the grain consolidation model, which was extended to take into account interfacial effects. The permittivity at high (megahertz) frequencies can be understood by using simple mixing laws. We also propose an equivalent circuit for the electrical properties of a liquid-impregnated porous solid.

1. Introduction

Despite considerable efforts the dielectric properties of impregnated porous media are still poorly understood. The dielectric properties of porous materials are of importance in many circumstances, and it is desirable to obtain a thorough understanding of these phenomena. We mention here electrical insulation systems, where it is obvious that the dielectric properties are of interest, but dielectric measurements are also often used as a non-destructive tool for diagnosing, e.g., excess humidity in cement [1].

In order to facilitate the study of impregnated porous solids, one often uses artificial "rocks", e.g., sintered glass spheres. Such a porous material can be impregnated with a liquid, e.g., salty water.

The construction of artificial rocks facilitates the study of multiphase systems. It is desirable that the solid component is as homogeneous as possible and does not consist of grains of different materials (as can be the case for natural sedimentary rock). Furthermore, the results are easier to interpret if both the solid and the pore fluid do not display any intrinsic dielectric relaxations. Unless one wants to study how such relaxations are influenced by the presence of other phases, materials such as polypropylene, which has very low dispersion, is of practical use for fabrication of "artificial rocks".

In a series of articles [2–7], we have discussed various subjects related to the dielectric behaviour of liquid-impregnated porous solids. In this article we present a thorough theoretical and experimental study of the dielectric properties of porous solids consisting of glued sand grains or of sintered polypropylene. Experimentally, we study the dependence of the permittivity and alternating-current (a.c.) conductivity on frequency, porosity and liquid conductivity. The results are interpreted in the framework of the grain consolidation model (GCM). In this model, we have included the effects of the electrochemical double layer at the pore interfaces. We aim at an integrated approach to the frequency dependence of porous materials and identify various relaxation mechanisms.

In particular, we discuss four aspects of this field:
1. the high-frequency permittivity, including comparisons with mixture formulae;
2. model calculations of the dielectric spectrum, the implications of such calculations and comparisons with experiments;
3. the low-frequency relaxation due to the electrochemical double layer and its dependence on porosity, grain size distribution and microgeometry;
4. the arcs found in so-called Argand diagrams, including the situation where we have double-layer effects as well as electrode effects.

The materials that we have studied were artificial sandstones impregnated with salty water, and polypropylene samples impregnated with an organic liquid containing ions.

2. Theory

2.1. Relaxation processes

2.1.1. Double-layer effects

It has been shown, in the case of liquid-impregnated porous solids, that the low-frequency permittivity can

0022–2461

have very large values, which cannot be dismissed as "electrode effects" [2, 8, 9]. We have shown earlier that this may be explained by diffusion effects in the electrochemical double layer at the solid–liquid boundary. The equation, originally obtained as an approximation for dilute suspensions of spherical particles in an electrolyte [10, 11],

$$\varepsilon' = \frac{A}{(1+\omega\tau)[1+(\omega\tau)^{0.5}]} + \varepsilon_\infty$$

$$\sigma_{a.c.} = \frac{A\omega\varepsilon_0(\omega\tau)^{0.5}}{(1+\omega\tau)[1+(\omega\tau)^{0.5}]} + \sigma_0 \qquad (1)$$

$$= \frac{\Delta\sigma(\omega\tau)^{0.5}}{(1+\omega\tau)[1+(\omega\tau)^{0.5}]} + \sigma_0$$

was found to give good agreement with experimental data [4, 5]. Here, ε_∞ is the value of the permittivity far above the relaxation described by Equation 1 (but below any other relaxations that may exist), σ_0 is the conductivity at zero frequency (far below the relaxation) and $\Delta\sigma$ is the difference between the a.c. conductivities at frequencies above and below the relaxation. The values of A are the same for both ε' and $\sigma_{a.c.}$. For dilute suspensions of spherical particles of radius a, τ is roughly $a^2/2D$, where D is the diffusion constant in the electrolyte. We have recently [4] studied the behaviour of the low-frequency relaxation for artificial sandstones and the dependence on the conductivity of the liquid. We found that the permittivity's frequency dependence had a strong resemblance to the prediction of Equation 1. One important discovery was that the value of τ was much lower than predicted in theories for dilute suspensions. This was also found in the theoretical work on non-dilute suspensions by Shilov and Borkovskaya [12]. We also found a dependence of τ on the conductivity of the liquid.

Equation 1 may give good agreement with experimental data for the apparent permittivity of an inhomogeneous sample, but it does not contain any inherent information related to the microstructure of the sample. Nor has it been theoretically justified for the case of an impregnated porous solid. We note that τ, as well as the parameter A, should be dependent on the grain size (or grain size distribution), on the pore structure of the sample, and on the solid and the liquid used. Furthermore, we note that Equation 1 cannot be valid at all frequencies for the composite material as a whole, but only for the double layer. Another relaxation which arises because of the heterogeneity of the sample is obtained at higher frequencies. This relaxation is not accounted for in Equation 1. Finally, as we have shown in a previous article [13], models of porous materials can be used to estimate the variation in the electric field within the heterogeneous material. As the double layer can influence the distribution of the electric field, it is of interest to include this layer in model calculations, however.

2.1.2. Maxwell–Wagner polarizaton

In an inhomogeneous material, where at least one of the components is conducting (and where the components do not have exactly the same electrical properties), a dielectric relaxation will occur owing to the inhomogeneity of the sample [14]. This relaxation is called the "Maxwell–Wagner" relaxation. Formulae for the dielectric constant and for the conductivity in the limits of high and low frequencies, as well as the formula for the relaxation time can be found, for example, in [15], for the case of one material consisting of spheres, dilutely suspended in the other material. Blum *et al.* [15] measured the dielectric dispersion of polybead carboxylate microspheres and obtained a low-frequency relaxation, which was attributed to double-layer effects. For high frequencies, they obtained another relaxation, which was attributed to Maxwell–Wagner polarization.

2.1.3. Electrode effects

The conduction of charge through the interface between an electrode and an ionic conductor (such as an ion-containing liquid) is not ideal. The penetration of charge can be more or less blocked (the discharge of ions is performed at a finite rate). Adsorption of ions onto the electrode surface will also influence the charge transport. In general, these limitations can be modelled as a frequency-dependent impedance, in series with the sample [16]. These effects may become dominant at low frequencies and high values of the fluid conductivity [4].

2.2. Direct-current conductivity and analogy with low-frequency permittivity

The dependence of the apparent direct-current (d.c.) conductivity of a porous non-conducting solid, impregnated with a conducting liquid and having an interface conductivity has been thoroughly studied [17–20]. Johnson and co-workers [17, 18] found that, when the conductivity of the pore fluid, σ_f, is high, the following formula applies:

$$\sigma_{eff} = \frac{1}{F}\left(\sigma_f + \frac{2\Sigma_s}{\Lambda}\right) \qquad (2)$$

Here Σ_s is the interface conductivity, Λ is a geometrical parameter that can be described as an "effective pore radius" and F is the so-called electrical formation factor which, in the presence of interface conduction, can be defined as

$$F = \lim_{\sigma_f \to \infty}\left(\frac{\partial\sigma_f}{\partial\sigma_{eff}}\right) \qquad (3)$$

where σ_{eff} is the effective conductivity of the composite. For low values of σ_f, another expression is obtained [21], which is still linear in $\sum_s$. Asymptotically, there will be "contributions" to the total conductivity from interface conduction that are proportional to the interface conductivity. The ratio of the proportionality coefficients at high and low values

of σ_f becomes

$$K = \frac{\left(\int |\boldsymbol{e}_0(\boldsymbol{r})|^2 \, dS\right)}{\left(\int |\boldsymbol{E}_0(\boldsymbol{r})|^2 \, dS\right)} \tag{4}$$

where $\boldsymbol{E}_0$ and $\boldsymbol{e}_0$ are the electric fields in the high-σ_f limit and low-σ_f limit, respectively, and the integration is performed on the pore–solid interface.

For any value of σ_f, we can write [7]

$$\sigma_{app,\,ic} = \frac{2c\Sigma_s}{F\Lambda} \tag{5}$$

Here c is a parameter that is unity for high values of σ_f and approaches K for low values of σ_f. The subscript ic is used to denote the contribution from interface conduction. We noticed [7] that the parameter c should exhibit a weak porosity dependence.

By analogy with Equation 5, we proposed [7] an approximate relation for the low-frequency permittivity. Provided that the high values of the permittivity are due to interface effects within the "bulk" of the inhomogeneous sample, we proposed that

$$\varepsilon_{app} = \frac{2cE_s}{F\Lambda} \tag{6}$$

where E_s is an "effective surface permittivity".

It is here assumed that E_s may depend on frequency, but that it does not vary among samples made of the same materials. The parameter Λ also occurs in a relation between the formation factor and the fluid permeability:

$$k = \frac{\Lambda^2}{8F} \tag{7}$$

This means that data for both the formation factor and the fluid permeability can be used to estimate Λ [3].

2.3. Mixing formulae

For composite media, different kinds of mixture law have been proposed for the effective dielectric constant, ε_{eff}. (For a more thorough review of such laws, and their properties, see, for example, [22, 23].) The two simplest cases arise when the components form layers, either parallel to the applied electric field, which is given by

$$\varepsilon_{eff} = \varphi_1\varepsilon_1 + \varphi_2\varepsilon_2 \tag{8}$$

or in a series combination, which is given by

$$\frac{1}{\varepsilon_{eff}} = \frac{\varphi_1}{\varepsilon_1} + \frac{\varphi_2}{\varepsilon_2} \tag{9}$$

Here ε_1 and ε_2 are the dielectric constants of materials 1 and 2, respectively, and φ_1 and φ_2 their volume fractions. These two expressions can be generalized to

$$\varepsilon_{eff}^{\beta} = \varphi_1\varepsilon_1^{\beta} + \varphi_2^{\beta}\varepsilon_2 \tag{10}$$

Special values of β include the complex refractive index model (CRIM) [24] as given by

$$\varepsilon_{eff}^{1/2} = \varphi_1\varepsilon_1^{1/2} + \varphi_2^{1/2}\varepsilon_2 \tag{11}$$

or the relation proposed by Looyenga [25] and by Landau and Lifshitz [26], which is

$$\varepsilon_{eff}^{1/3} = \varphi_1\varepsilon_1^{1/3} + \varphi_2^{1/3}\varepsilon_2 \tag{12}$$

as well as the relation of Lichtenecker [27] :

$$\ln \varepsilon_{eff} = \varphi_1 \ln \varepsilon_1 + \varphi_2 \ln \varepsilon_2 \tag{13}$$

Among effective-medium theories, we can mention the Bruggeman formula [28]

$$\varphi_1\frac{\varepsilon_1 - \varepsilon_{eff}}{\varepsilon_1 + 2\varepsilon_{eff}} + \varphi_2\frac{\varepsilon_2 - \varepsilon_{eff}}{\varepsilon_2 + 2\varepsilon_{eff}} = 0 \tag{14}$$

and that of Maxwell Garnett [29] :

$$\frac{\varepsilon_{eff} - \varepsilon_{host}}{\varepsilon_{eff} + 2\varepsilon_{host}} = \varphi_{guest}\frac{\varepsilon_{guest} - \varepsilon_{host}}{\varepsilon_{guest} + 2\varepsilon_{host}} \tag{15}$$

Contrary to the earlier expressions, this theory is asymmetric, treating one of the materials (indicated by the subscript guest) as a "guest" medium, forming spherical particles completely surrounded by the other material (indicated by the subscript host), the "host" medium. This is also the case for the differential effective-medium (DEM) theory of Bruggeman [28] and Hanai [30]:

$$\frac{\varepsilon_{guest} - \varepsilon_{eff}}{\varepsilon_{guest} - \varepsilon_{host}} = (1 - \varphi_{guest})\left(\frac{\varepsilon_{eff}}{\varepsilon_{host}}\right)^{1/3} \tag{16}$$

This equation has been extended by Boned and Peyrelasse [31] to the situation where the inclusions of guest material are covered by an interface layer. Their result applies to rotationally symmetric randomly distributed ellipsoids:

$$1 - \varphi_{guest} = \left(\frac{\varepsilon_{host}}{\varepsilon_{eff}}\right)^{3d}\left(\frac{\varepsilon_{host} - r}{\varepsilon_{eff} - r}\right)^{3K_1}\left(\frac{\varepsilon_{host} - s}{\varepsilon_{eff} - s}\right)^{3K_2} \tag{17}$$

where

$$d = \frac{A(1 - 2A)}{2 - 3A} \qquad K_1 = \frac{Y - Xr}{\Delta^{1/2}} \qquad K_2 = \frac{Xs - Y}{\Delta^{1/2}}$$

$$s = \frac{[\varepsilon_{1a}(3A - 1) + 3A\varepsilon_{1b}] - \Delta^{1/2}}{2(3A + 1)}$$

$$r = \frac{[\varepsilon_{1a}(3A - 1) + 3A\varepsilon_{1b}] + \Delta^{1/2}}{2(3A + 1)}$$

$$\Delta = \varepsilon_{1a}^2(3A - 1)^2 + 9A^2\varepsilon_{1b}^2 - 2\varepsilon_{1a}\varepsilon_{1b}(9A^2 - 3A - 4)$$

$$X = \frac{A(9A - 5)}{3A - 2} \qquad Y = \frac{2\varepsilon_{1a}(2A - 1)^2 + \varepsilon_{1b}A^2}{3A - 2}$$

$$\varepsilon_{1a} = \varepsilon_{layer}$$

$$\left(1 + \frac{\varepsilon_{core} - \varepsilon_{layer}}{\varepsilon_{layer}/f + (\varepsilon_{layer} - \varepsilon_{core})[H_a(0) - H_a(-G)]}\right) \tag{18}$$

and analogosly for ε_{1b},

$$H_l(u) = \frac{ab^2}{2}\int_u^\infty \frac{d\lambda}{(\lambda + g_l^2)D_\lambda}$$

$$D_\lambda = [(\lambda + a^2)(\lambda + b^2)^2]^{1/2} \quad (19)$$

The external surface of the interface layer is described by

$$\frac{x^2}{a^2} + \frac{y^2}{b^2} + \frac{z^2}{b^2} = 1 \quad (20)$$

and the surface of the solid inclusions by

$$\frac{x^2}{a^2 - G} + \frac{y^2}{b^2 - G} + \frac{z^2}{b^2 - G} = 1 \quad (21)$$

Also, f is the volume fraction of solid divided by the volume fraction of interface layer, $g_a = a$, $g_b = b$ and A is the depolarization factor in the direction of the applied field. For a sphere, $A = \frac{1}{3}$.

3. Model calculations

3.1. General considerations

In a previous paper [2], we presented high values of the permittivity at low frequencies for artificial sandstone samples, made of sand grains and small amounts of epoxy. We interpreted these high values as due to diffusion effects at the solid–liquid interface. We succeeded in using a simple model for predicting the dielectric properties of brine-saturated porous solids and obtained reasonable agreement with experimental results.

This model, the GCM [32–34], treats in its simplest form the solid material as "grains" of truncated equal-sized spheres, placed on a lattice (Fig. 1a). The size of the spheres is determined from the lattice used and the selected porosity. More complicated versions of this model exist, with grains of different sizes or randomly placed [33].

In our version of the model [2, 35], we added a third phase, corresponding to the electrochemical double layer (Fig. 1b). As a crude model for the dielectric properties of this third phase, we used the equivalent circuit shown in Fig. 1c, where W denotes a Warburg impedance. In [2], we assumed no specific interface conductivity; instead, we assumed that the interface layer had the same high-frequency properties as the bulk liquid.

In this paper, we use a more realistic model for the electric properties of the interface layer, and assume that it can be described by Equation 1. One drawback of the GCM in the simplest version is the regular structure of the composite material. One possible way to simulate a more disordered structure would be to use a DEM theory including an interface layer, such as Equations 17–21. One drawback of the DEM theory is that only one phase, namely, the host medium, is continuous. In a real porous solid, such as a sandstone, both the solid and the pore fluid are continuous throughout the material. In particular, the double layer at the interface should be continuous.

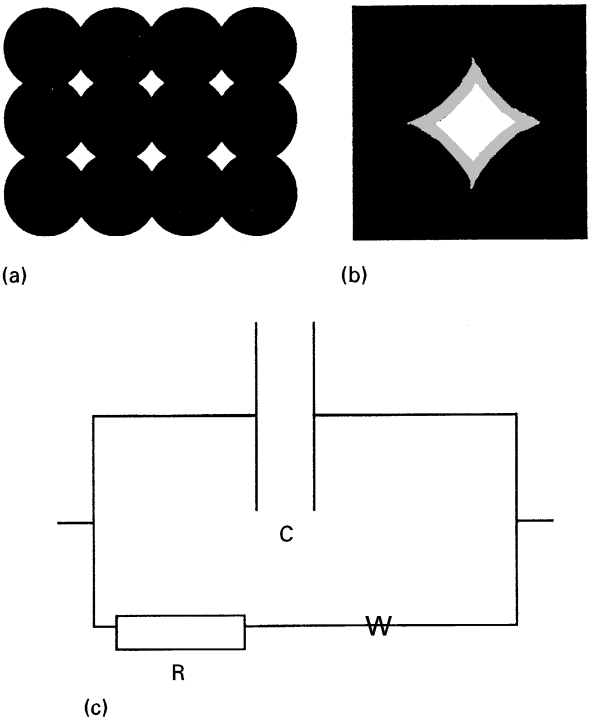

Figure 1 (a) Cross-section of one layer in the s.c. lattice for the GCM. (b) The model of the interface and double layer (not necessarily drawn to scale). (c) The equivalent circuit used to model the properties of the interface layer in our earlier article [2].

3.2. Extended grain consolidation model

To calculate the apparent dielectric properties of the composite, we used the method that was developed by Shen *et al.* [34] for the GCM. Since the solid phase is considered to consist of equal grains on a regular lattice we can Fourier transform the geometry and solve Maxwell's equations in Fourier space. By dividing the electric field in two parts according to

$$\boldsymbol{E} = \boldsymbol{E}_1(\boldsymbol{r})\theta_1(\boldsymbol{r}) + \boldsymbol{E}_2(\boldsymbol{r})\theta_2(\boldsymbol{r}) \quad (22)$$

where θ_1 has the value 1 in material 1 and 0 in material 2 (and vice versa for θ_2), fewer Fourier terms are needed for achieving good convergence. We write the Fourier series

$$\boldsymbol{E}_1(\boldsymbol{r}) = \sum_m \boldsymbol{C}_{1m}\exp^{(i\boldsymbol{b}_m\cdot\boldsymbol{r})} \quad \theta_1(\boldsymbol{r}) = \sum_m \mathrm{T}_{1m}\exp^{(i\boldsymbol{b}_m\cdot\boldsymbol{r})} \quad (23)$$

(and analogously for $\boldsymbol{E}_2(\boldsymbol{r})$ and $\theta_2(\boldsymbol{r})$). Maxwell's equations are then written as

$$\boldsymbol{b}_n \times \sum_\alpha \sum_m T_{\alpha n-m}\boldsymbol{C}_{\alpha m} = \boldsymbol{0} \quad \boldsymbol{b}_n \cdot \sum_\alpha \sum_m \varepsilon_\alpha T_{\alpha n-m}\boldsymbol{C}_{\alpha m} = 0 \quad (24)$$

where α denotes summation over the different phases and $\boldsymbol{b}_n$ represent vectors in reciprocal space (in principle, Equation 24 should be valid for all possible vectors $\boldsymbol{b}_n$).

The effective ε in the $\boldsymbol{j}$ direction (if the composite is anisotropic) is obtained from

$$\varepsilon_{\mathrm{eff},j} = \frac{1}{E_{0j}}\sum_\alpha \sum_m \varepsilon_\alpha T_{\alpha 0-m}(\boldsymbol{C}_{\alpha m}\cdot\boldsymbol{e}_j) \quad (25)$$

where E_{0j} is the component in the j direction of the applied field and $\boldsymbol{e}_j$ is the unit vector in the j direction.

We extended this method to three-phase systems and to complex frequency-dependent properties [2, 35]. We also used the method for estimating the maximum electric field within the different phases in a composite subjected to an externally applied field [13]. As in [2], we truncated the Fourier expansion after the second-order term in the calculations presented here.

For the DEM theory, we use the equations of Boned and Peyrelasse [31], Equations (17)–(21), assuming spherical grains with an interface layer of constant thickness.

3.3. Calculation conditions

3.3.1. General remarks

To compare the results of the model calculations with experimental data, we specified the parameter values used in the calculations so that they corresponded to a particular measurement. As described in Section 3.3.3, we used values of an intercept in a linear fit of conductivity data to model the relaxation amplitude. However, for the measurements on polypropylene samples [5], we were not able to obtain such intercepts, and we have accordingly only performed model calculations for sandstones. (The dielectric spectrum of the polypropylene samples were qualitatively very similar to the sandstone spectra.) We assumed a fairly low value of the liquid conductivity, in order to render any electrode effects negligible.

In the GCM, we considered the material to consist of spherical "grains" forming a regular lattice. The porosity was assumed to be the same as for the actual sample. We used a simple-cubic (s.c.) lattice in most of the calculations, since this would give a geometry where the solid particles were in contact but, for comparison, we also performed calculations using body-centred cubic (b.c.c.) and face-centred cubic (f.c.c.) lattices (in these two lattices, the particles are not in contact at the values of the porosity used). Also, for the DEM theory, we assumed the porosity to be the same as that of the actual sample.

We let the diameter of the grains be 0.25 mm (the median grain diameter of the actual sample) and assumed the thickness of the interface layer to be one Debye length, l_D, (using an estimated value of the diffusion constant, D, of 2.0×10^{-9} m^2 s^{-1}, which was also used by Chew and Sen [10]). This would yield a value of l_D of 38 nm for the fluid conductivity 1 mS m^{-1}, and an l_D of 1.2 nm for the fluid conductivity 1 S m^{-1}. The value of ε' of the bulk liquid was assumed to be 80, and the conductivity of the bulk liquid was assumed to be the same as that of the liquid used for impregnation of the samples in the experiments. The permittivity of the grains was assumed to be 4.3 corresponding to quartz [36]; the grains were not assumed to have any electrical conductivity.

We assumed that the dielectric properties of the interface layer could be described by Equation 1, where we put ε_∞ equal to the permittivity of the bulk liquid (80). (σ_0 is discussed below.) By using a differentiation technique, as described in [4], we were able to estimate the relaxation time, τ, from experimental spectra. We assume that the amplitude, A, is the same both in the equation for the permittivity and in the equation for the a.c. conductivity of the interface layer.

3.3.2. The value of σ_0

Theories of dilute colloidal suspensions, such as the theory of DeLacey and White [37], predict a much higher value of σ_0 than of the conductivity increment, $\Delta\sigma$, due to the relaxation and the ratio, $\sigma_0/\Delta\sigma$, of these two parameters, increases with increasing liquid conductivity. For the particle sizes (median diameter, 0.25 mm) and the liquid conductivities (around 10 mS m^{-1} of main interest in our simulations) it would appear as if the ratio $\sigma_0/\Delta\sigma$ were so high that the effect of the relaxation on the a.c. conductivity would be negligible. However, it must be stressed that theoretical results for dilute suspensions are not necessarily valid for high volume concentrations. The calculations of Shilov and Borkovskaya [12] on non-dilute suspensions of spherical particles imply that $\Delta\sigma$ should increase with increasing volume fraction of solid. As will be shown in this paper, the emergence of contacts between the solid particles (and their double layers) increases the relaxation strength substantially. As we have shown previously, the low-frequency relaxation has a pronounced effect on the frequency dependence of the a.c. conductivity [3], and this dependence cannot be dismissed as electrode effects [2]. We can thus assume that the low-frequency relaxation has a non-negligible effect on the a.c. conductivity for a liquid-impregnated porous medium and that $\Delta\sigma$ should be larger than σ_0, maybe by several orders of magnitude.

The value of σ_0 is difficult to determine, as electrode effects become dominant at frequencies higher than where $\sigma_{a.c.}$ has settled to a constant low-frequency value. It must be stressed that σ_0 by no means equals zero, even if it is negligible. We have chosen to let σ_0 have the same value as the conductivity, σ_f, of the bulk liquid. For low values of σ_f (on which we concentrate), $\Delta\sigma \gg \sigma_f$ but, for higher values of σ_f, that does not hold. Note that $\Delta\sigma$ is not the relaxation amplitude in the apparent conductivity of the composite material, but the corresponding amplitude for the double layer only (or for an idealized interface layer that is homogeneous and isotropic and has the same influence on the effective properties of the composite as the real double layer).

3.3.3. Values of the amplitude A

As an initial possibility, we choose $A = 0$, to study the dispersion in the absence of double-layer effects. In this paper, we denote such a choice as "no interface conductivity". For $A > 0$, the calculated a.c. conductivity for frequencies above the double-layer relaxation will be increased, as compared with calculations assuming $A = 0$. In a previous paper [3], we noted that the a.c. conductivity as a function of frequency displayed a "plateau" (this is also shown in this article

later in Figs 2 and 3). The value at the plateau was not directly proportional to the conductivity of the pore fluid. Still, a linear dependence was found, but with a finite intercept value in the limit $\sigma_f \to 0$. As we shall see later, such a plateau is obtained also in our model calculations when $A > 0$. One could thus argue that a suitable choice for A would be a value that would yield an increase in conductivity at the "plateau" that is equal to the "intercept" found in the $\sigma_f \to 0$ limit in the experiments. For simplicity, we call such a choice "low interface conductivity". For a given value of A, the increase in a.c. conductivity at the plateau is dependent on the model used. Accordingly, we use different values of A for the GCM and for the DEM model. These values were obtained by systematically varying the value of A in the model calculations, and comparing the results with the case $A = 0$.

Another choice would be to use a value corresponding to the value of interface conductivity found in the previous article [3] (it is in the range 0.1–0.3 μS). The high-frequency conductivity of the interface layer is then obtained as Σ_s/l_D, where Σ_s is the measured surface conductivity and l_D is the assumed thickness of the layer (one Debye length). This value would be higher than the first choice owing to the deviations from spherical shape of the grains, the non-regularity of the grain packing and the rough grain surfaces. In this paper, we call this value "high interface conductivity". The reason for using two different values in the simulations is that the geometry of a real porous medium is more complicated than in the simulations, yielding a higher formation factor. The higher formation factor decreases the influence of the interface relaxation on the apparent dielectric properties of the composite material. Note that an increased relaxation strength, $\Delta\sigma$, as well as an increased zero-frequency conductivity, $\sigma_0 - \sigma_f$ of the double layer will increase the effective conductivity of the composite. If we assume a value of $\sigma_0 > \sigma_f$, the value of A has to be decreased in the simulations in order to fit the experimental data.

3.3.4. Remark on the calculation conditions

It should be remarked that almost all the parameters used (porosity, fluid conductivity, etc.) have been measured separately. The only unknown parameters are the value of σ_0 (whose influence we so far consider negligible) and the relaxation time, τ, which thus could be viewed as an "adjustable parameter". Yet, it should be remarked that we obtained the value of τ used only from the shape of the log ε' versus log(frequency) curve and not from the amplitude of the curve. The amplitude, A, in Equation 1 is obtained from measured values of the conductivity and from the value of τ.

4. Experiments

4.1. Materials

The samples used in the experiments described in this paper are of two different types: artificial sandstones and porous polypropylene samples.

4.1.1. Artificial sandstones

These samples have been described in other papers [3, 38, 39]. They were made of Danish beach sand, to which small amounts of epoxy (about 3 vol%) had been added. The samples were deliberately constructed to have a grain size distribution that was log-normal by relative weight. The median grain diameter was 0.25 mm. Four different series of samples were constructed, having the standard deviations in the log-normal distribution 0.25, 0.50, 0.75 and 2.0 (called the S1, S2, S3 and S4 series, respectively) according to the ϕ scale (the ϕ scale is defined as $\phi = -\log_2 d_g$, where d_g is the grain diameter in millimeters). Before the epoxy was cured, the samples were subjected to pressures of 0.2, 2, 5 or 10 MPa. Some samples subjected to 10 MPa were also subjected to vibrations before curing. The samples subjected to 0.2 MPa are denoted by an E (as in sample S3E) and the samples subjected to 10 MPa and vibrations are denoted by an *A*. This preparation method yielded samples with porosities in the range of 0.19–0.46.

4.1.2. Polypropylene samples

These samples have been described in [5]. Polypropylene beads (Hostalen HH1414), manufactured by Hoechst, were packed and heated to 165 °C. The original distribution of grain sizes was found to be roughly log-normal by relative weight, with a median diameter of about 0.2 mm and a standard deviation of about 0.5 on the ϕ scale. For some samples, we deliberately altered the grain size distribution to attain the median 0.25 mm and standard deviation 0.75 on the ϕ scale.

4.1.3. Pore liquids

Two different kinds of liquid have been used: deionized water, and a mixture of mono benzyl toluene (MBT) and dibenzyl toluene (DBT), manufactured by Prodelec.

We added different amounts of ions to both liquids. To the water, sodium chloride was added (we used water with conductivity values between 0.008 and 1.2 S m^{-1}); to the MBT–DBT, we added tetraisoammyl ammonium picrate (here, the highest conductivity attained at room temperature was 90 nS m^{-1}).

4.2. Measurement techniques

Measurements on brine-impregnated sandstone samples were performed between 5 Hz and 13 MHz using an HP4192 A impedance analyser. The instrument was calibrated at 100 kHz.

Low-frequency measurements (1 kHz down to 0.1 mHz) were performed on the measurement system of ABB Corporate Research in Västerås [40]. This equipment was used for the impregnated polypropylene samples, as well as for measurements on samples in vacuum, together with an HP 4284 A *LCR* analyser, which was used for frequencies up to 1 MHz. For the HP 4284 A, 'Open' and 'Closed' calibrations were

performed, as well as 'Load' calibration for 100, 200 and 480 kHz.

The samples were placed in a test cell between brass electrodes. We used a guard electrode to eliminate the influence of conduction on the external surface of the sample. The electrodes were mounted on plastic screws, which enabled us to measure on samples with different thicknesses (the thickness varied between 3 and 18 mm) and to achieve a good contact between the sample and the electrodes. The samples were impregnated in a vacuum chamber which was evacuated to 0.1 Torr before letting the impregnation liquid into it.

All measurements referred to in this paper were performed at room temperature.

5. Results and discussion

5.1. Frequency dependence for unimpregnated porous solids

In Figs 2 and 3, we show the frequency dependence of the permittivity and of the a.c. conductivity for an artificial sandstone sample and a polypropylene sample, respectively. The porosities were 46% and 35%, respectively; the samples were not impregnated and they were placed in vacuum during the measurements. We note that the polypropylene sample has very low dispersion. The dispersion of the sandstone is larger, especially towards low frequencies. There also appears to be a small relaxation around 10 kHz for the sandstone. The conductivity of the sandstone is low, but it increases towards higher frequencies, approximately as a power law, $\sigma_{a.c.} \propto \omega^n$, with $n \approx 0.7$–0.8. The conductivity of the polypropylene at low frequencies appears to be lower than the detection limit of the measurement system. (In fact, the measured conductivities at the lowest frequencies for the polypropylene are sometimes negative, and we chose to plot the modulus of the measured value in the logarithmic plot.)

5.2. Porosity dependence for unimpregnated porous solids

The permittivity at 480 kHz for artificial sandstone samples in vacuum is shown in Fig. 4 as a function of the porosity. There is some scatter but no clear dependence on the grain size distribution. Yet, it is clear that the permittivity decreases when the porosity increases.

From the measured values of the porosity, and the known permittivity of vacuum (equal to 1), we can fit Equations 10–16 to the data to obtain estimations of the permittivity ε_{sand}, of the sand grains. Results from such computer fits are given in Table I, where we also

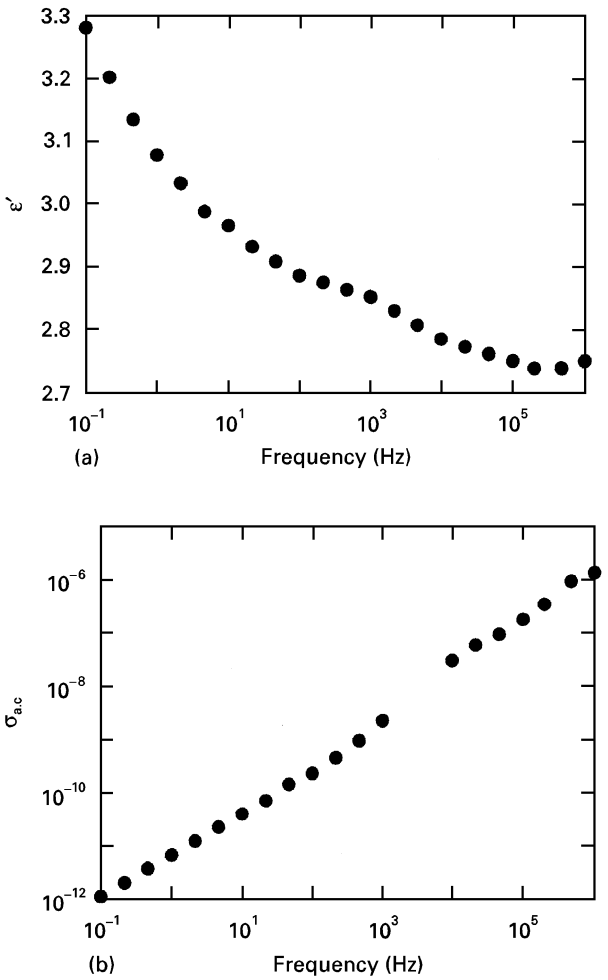

Figure 2 (a) The permittivity and (b) the a.c. conductivity of an artificial sandstone sample as a function of frequency. The porosity was 46% (sample S2D).

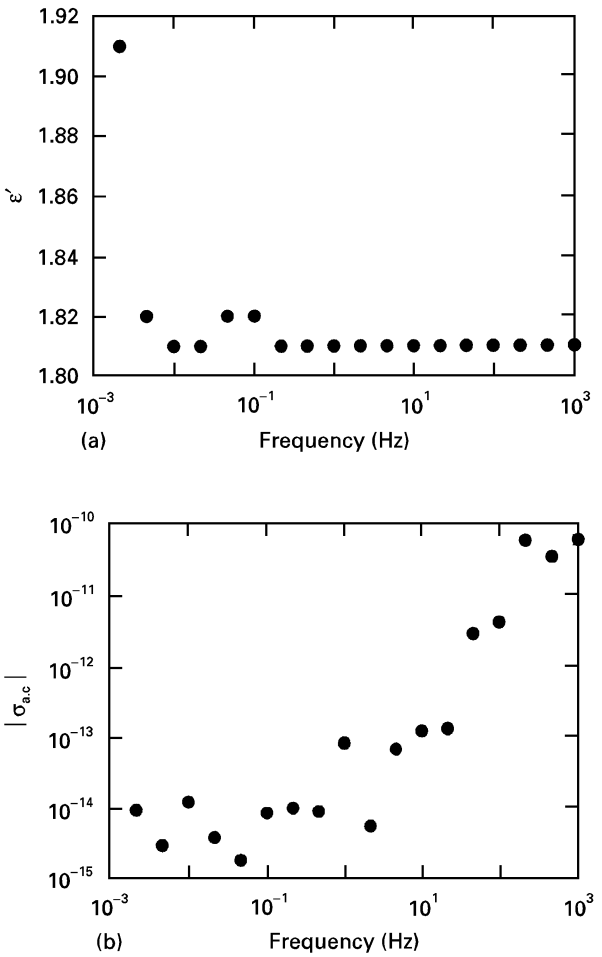

Figure 3 (a) The permittivity and (b) the a.c. conductivity of a polypropylene sample as a function of frequency. The porosity was 35%.

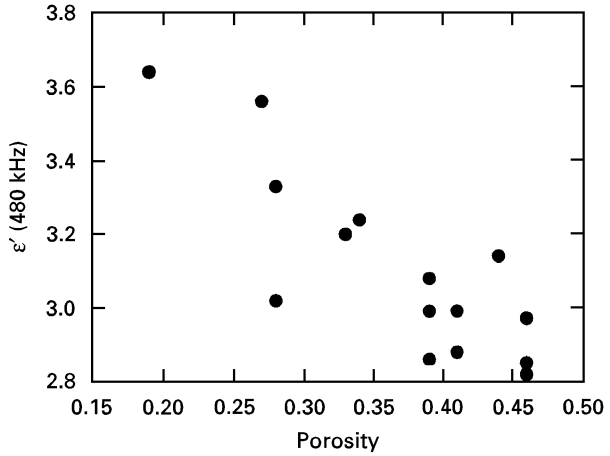

Figure 4 The measured dielectric constant at 480 kHz for unimpregnated artificial sandstone samples as a function of porosity.

give the correlation coefficient, R. (It should be noted that, in these fittings, we have used the porosity as the dependent variable, as the effective dielectric constant is not expressed explicitly in some expressions, such as the Bruggeman–Hanai expression, Equation 16.) The different equations yield varying predictions, but 5.0 appears to be a rather typical value for the equations having a high correlation coefficient. Note, however, that Equation 10, using β as an adjustable parameter, yields a value of $\varepsilon_{sand} = 4.5$.

These values can be compared with the value of about 4.3 for ε' for quartz at 30 MHz [36].

5.3. Frequency dependence of impregnated samples

In Figs 5 and 6, we show the dielectric spectrum of impregnated samples. In Fig. 5, two sandstone samples are shown (having different porosities), whereas two polypropylene samples are displayed in Fig. 6 (having different porosities and different pore fluid conductivities). The dielectric properties of the two systems are qualitatively very similar. Towards low frequencies, the permittivity increases while the a.c. conductivity decreases. We attribute this to diffusion effects in the electrochemical double layer at the solid–liquid interface. At intermediate frequencies, the a.c. conductivity is almost independent of frequency. At the highest frequencies, the a.c. conductivity starts to increase. This increase is accompanied by a decrease in the permittivity. (This decrease in permittivity is not always clearly seen for the sandstone samples. We attribute this to the finite measurement resolution, since the ratio $\varepsilon''/\varepsilon'$ can be very high for the brine-impregnated samples in the frequency range where the decrease in permittivity occurs.) We had earlier speculated [3] that this increase in a.c. conductivity towards high frequencies might be an instrumentation artefact in the HP 4192 A since the manufacturer explicitly states that the accuracy is less for the highest frequency. However, since we obtained a similar increase (in another frequency range) for the

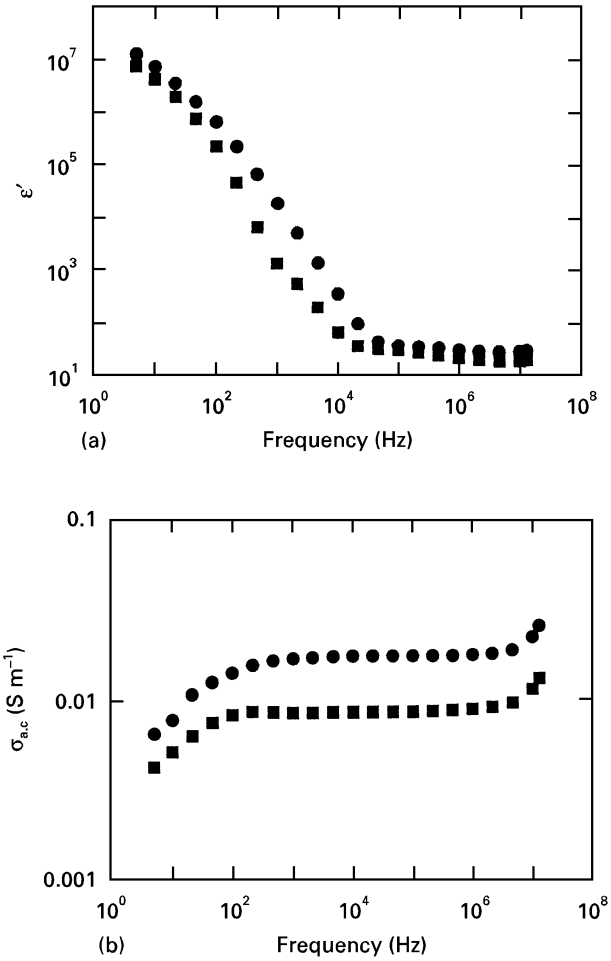

Figure 5 (a) The dielectric constant and (b) the a.c. conductivity of brine-impregnated artificial sandstone samples, having porosities of 46% (sample S1E) (●) and 28% (sample S2A) (■). The conductivity of the pore fluid was 63 mS m^{-1}.

TABLE I Comparison between different mixing formulae, giving their predictions of the permittivity of sand grains at 480 kHz, as well as the correlation coefficient, R, for the fits of the different formulae to the experimental data

Formula	Equation	Predicted ε'	R	Notes
Maxwell Garnett	15	4.75	0.83	sand as host
Maxwell Garnett	15	6.5	0.77	sand as guest
Bruggeman (symmetric)	14	5.1	0.79	
Bruggeman–Hanai	16	5.5	0.79	sand as guest
Bruggeman–Hanai	16	4.8	0.83	sand as host
Lichtenecker	13	5.9	0.78	
Looyenga, Landau and Lifshitz	12	5.1	0.81	
CRIM	11	4.8	0.83	
General β	10	4.5	0.84	$\beta = 0.82$

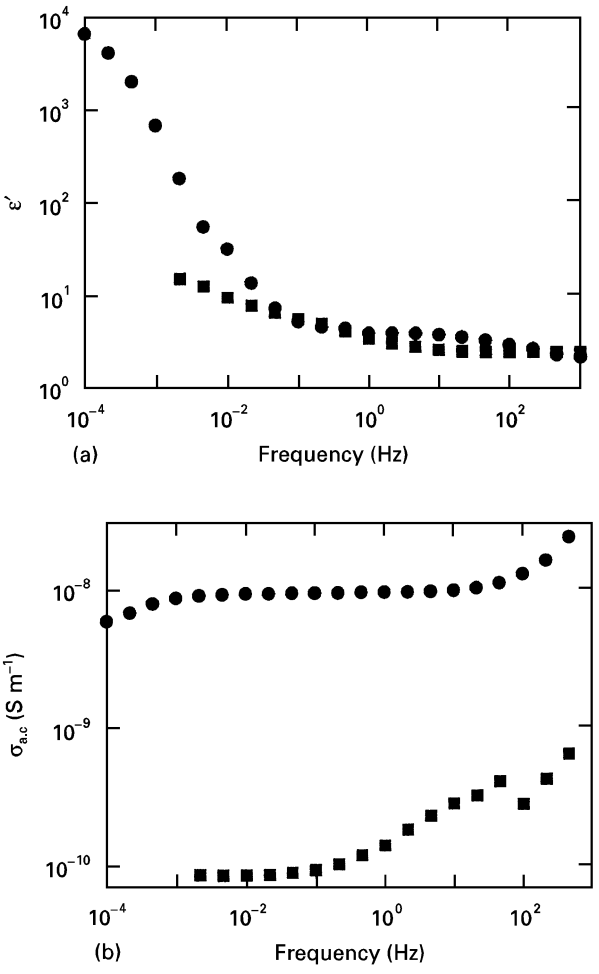

Figure 6 (a) The dielectric constant and (b) the a.c. conductivity of two MBT–DBT-impregnated polypropylene samples (●), porosity of 35%, fluid conductivity of 53 nS m^{-1}; (■), porosity of 25%, having the standard deviation 0.75 in the log-normal grain size distribution, fluid conductivity of 1.3 nS m^{-1}.

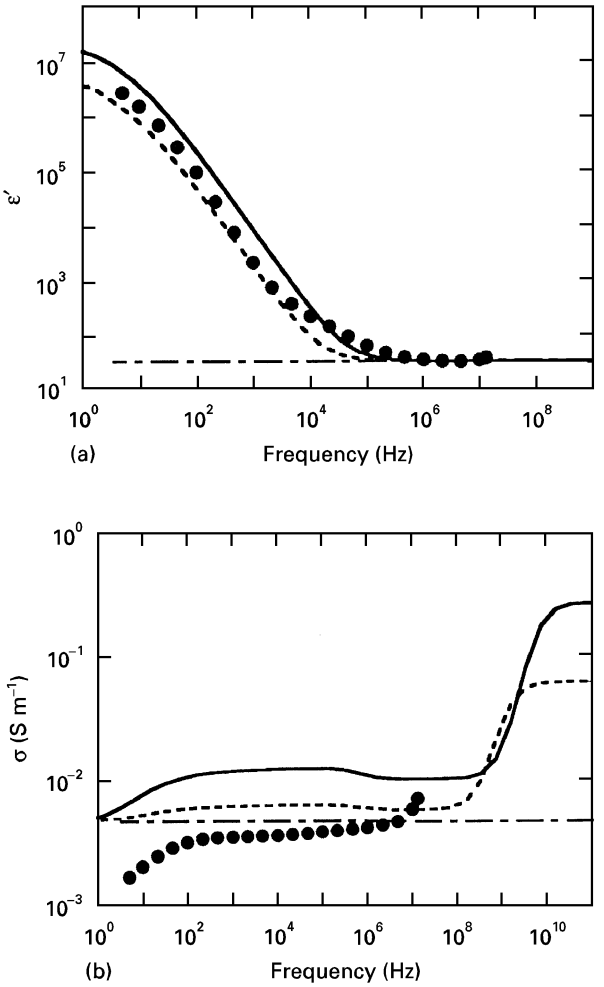

Figure 7 (a) Permittivity and (b) conductivity from experiments (●) and calculations using a s.c. lattice in the GCM with "high" interface conductivity (——), "low interface conductivity" (-----) and "no interface conductivity" (– – –). The porosity was 39%, the fluid conductivity was 12 mS m^{-1}, and the other parameters are as specified in the text.

polypropylene, it appears as if this increase is a real effect (it should be noted that we have also obtained such increases for artificial sandstones impregnated with MBT–DBT). Fig. 6b also shows that the increase in a.c. conductivity is shifted downwards in frequency as the conductivity of the pore fluid is decreased. We also note that Kenyon [41] and Holwech and Nøst [42] obtained relaxations in the same frequency range for sandstones and sintered glass bead samples, filled with salty water. The most probable explanation would be that the high-frequency relaxation is the Maxwell–Wagner-type relaxation that was seen by Blum *et al.* [15] for suspensions of polybead carboxylate microspheres. This is corroborated by the fact that the relaxation frequency is roughly the same as the theoretical value, using the formula for a dilute suspension of solid particles in a liquid [15].

5.4. Comparison with calculations

In Fig. 7, we show the experimental results for one sample together with data from the GCM simulations. Fig. 7a displays ε' and Fig. 7b the a.c. conductivity, $\sigma_{a.c.}$. The results from the DEM simulations are displayed in Fig. 8. The porosity used in the model simulations was 39%. The conductivity of the pore fluid was assumed to be 12 mS m^{-1}, yielding a Debye length of 11 nm. From experimental data, we obtained the value of $\frac{1}{30}$ s for the relaxation time τ.

For the assumed bulk liquid conductivity of 0.012 Sm^{-1}, the value of the conductivity in the interface layer was for "low interface conductivity" 5.4 S m^{-1} for the GCM calculation and 9.3 S m^{-1} for the DEM calculation.

The value of the interface conductivity for the pertinent sample found in [3] was 0.28 μS. For the "high interface conductivity" case, this gives a value of 25.4 S m^{-1} for the conductivity in an interface layer having a thickness of one Debye length.

We note that the GCM simulations with a higher interface conductivity than the bulk liquid conductivity yield an increase in $\sigma_{a.c.}$ at the highest frequencies. As discussed above, such an increase is also seen in the experimental data, while it is missing in the data for the simulation without interface conductivity. There is an increase also in the DEM conductivity, although it is smaller in amplitude. We also note that, for the DEM calculations, the high-frequency relaxation appears to be roughly in the same frequency range as

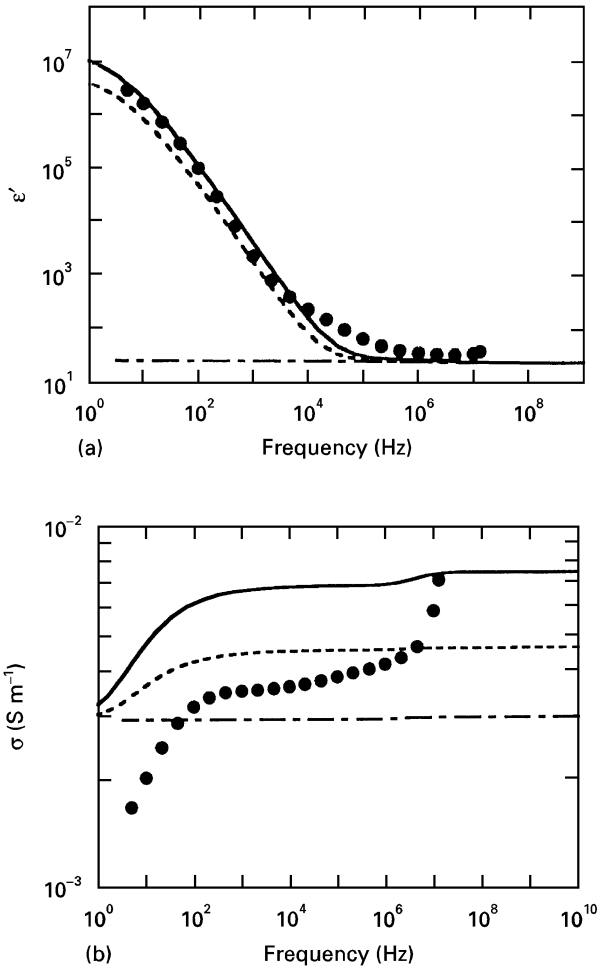

Figure 8 (a) Permittivity and (b) conductivity from experiments (●) and DEM calculations using "high" interface conductivity (——), "low interface conductivity" (-----) and "no interface conductivity" (– – –). Calculation parameters are as in Fig. 7.

the experimental data, whereas the GCM predicts a higher frequency for this relaxation. Note that the amplitude of the relaxation is strongly dependent on the value used for the conductivity in the interface layer, while the relaxation frequency appears to be more weakly dependent on this value. It should be remarked that we only observe one relaxation at high frequencies in the DEM results: it is therefore probable that the high-frequency relaxations found in experiments, as well as in GCM and DEM calculations are due to the same process. The high-frequency relaxation is not noticeable in the plot when we have no interface conductivity; however, we have previously shown [6] that a strong high-frequency relaxation can be obtained without assuming interface conductivity, but instead assuming a non-spherical grain shape. Since the sand grains can hardly be considered spherical in shape, it is probable that the use of ellipsoidal grain shapes in the DEM calculations would yield better agreement with experiments also for the size of the high-frequency relaxation. It should be stressed that the Maxwell–Wagner relaxation does not disappear in systems without surface conductivity; it only becomes negligibly small. A similar effect was obtained by Endres and Knight [43] for an effective-medium theory including an interface layer. The value of σ at the "plateau" in the medium-frequency range is much higher for the simulations with a surface conductivity than for the experimental data; this is due to the simplifications in the simulation (assuming truncated spheres of the same size with smooth surfaces produces a less obstructed path for ions in the bulk liquid, even in the DEM where this effect is also seen to some extent). The increase is due to enhanced conduction in the bulk fluid; for low and intermediate frequencies, we effectively obtain a larger frequency-independent conductivity term in the model calculations.

At low frequencies, we have very good agreement between the predictions of ε' from the simulations using a low interface conductivity and the experiments. It thus appears that σ_0 is of a different order of magnitude from $\Delta\sigma$, and that it can be neglected. For $\sigma_{a.c.}$, the decrease with decreasing frequency starts at roughly the same frequency in both simulations and experiments. As the values at the "plateau" are different, the experimental and theoretical values of the conductivity cannot be compared in detail at low frequencies.

We also find that, for the simulation using no interface conductivity, the low-frequency dependence of ε' does not agree with experiments. We are thus compelled to draw the conclusion that only the introduction of an interface conductivity can explain the measured dielectric frequency spectrum since we previously refuted the possibility of electrode effects as the cause of the high values of the permittivity [2, 4].

Around 10 kHz, there is disagreement between the simulated data and the experimental ε' values. In this region, tan δ (i.e., the ratio $\varepsilon''/\varepsilon'$) becomes very large, and the experimental values for ε' are therefore uncertain in this region, since the measurement resolution is finite. It should also be noted that the GCM predictions of the high-frequency value of ε' are in better agreement with the experimental values than are the DEM predictions.

For comparison, we have also performed simulations using b.c.c. and f.c.c. lattices. Results from such simulations are shown in Fig. 9, where we also compare with the results from GCM calculations using a s.c. lattice and results from DEM calculations. Now, we only compare calculations using "high interface conductivity". As stated above, in the b.c.c. and f.c.c. simulations the solid particles are no longer in contact for the porosity used. We note that the amplitude of the low-frequency relaxation is lower in these cases than for the simulations using a s.c. lattice. This is also the case for the DEM calculations. Similarly, the value of the parameter A used in the calculations using "low" interface conductivity had to be higher in the DEM theory than in the GCM to obtain the same increase in conductivity. This can be explained from the assumption in the DEM theory that the particles (and the interface layers) are not in contact, and the interface layer is not continuous throughout the material. The differences in low-frequency permittivity between the three different models where no contact is assumed between the grains are very small. In particular, the similarity between the results from GCM

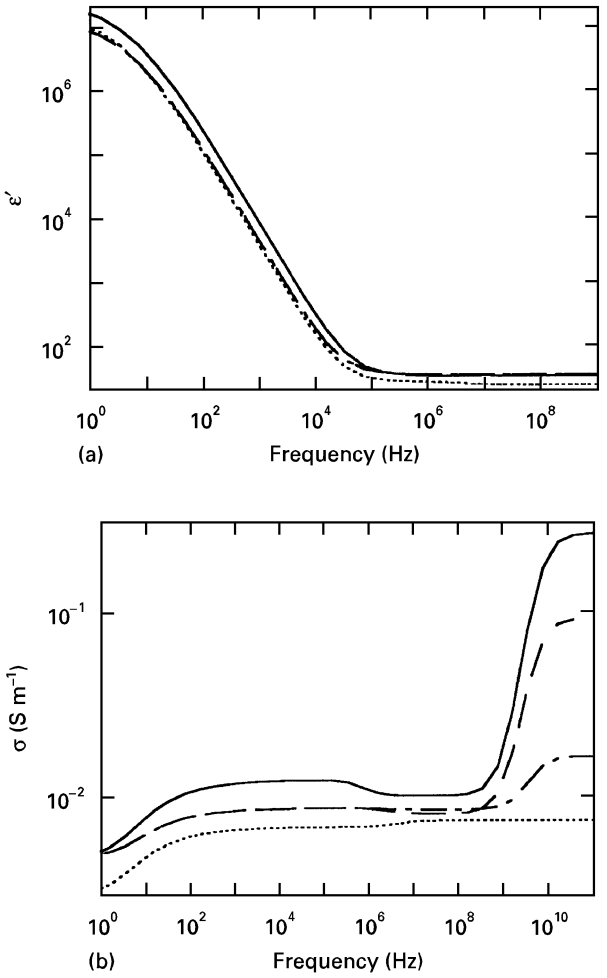

Figure 9 Results for (a) the permittivity and (b) the conductivity for the GCM using a s.c. lattice (——), using a b.c.c. lattice (— — —) and using a f.c.c. lattice (– – –), compared with results for DEM (-----). Parameters are as in Fig. 7. Note that the simulation results using a b.c.c. lattice and the results using a f.c.c. lattice are indistinguishable in (a) and fall onto the same curve.

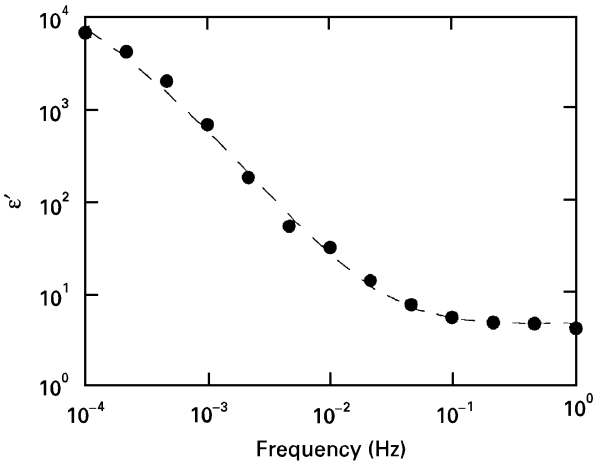

Figure 10 An MBT–DBT-impregnated polypropylene sample (data as in Fig. 6 for the sample having 35% porosity), and a computer fit to Equation 1 for low frequencies. The fit yielded the parameters $A = 34\,000$, $\tau = 1890$ s and $\varepsilon_\infty = 4.4$.

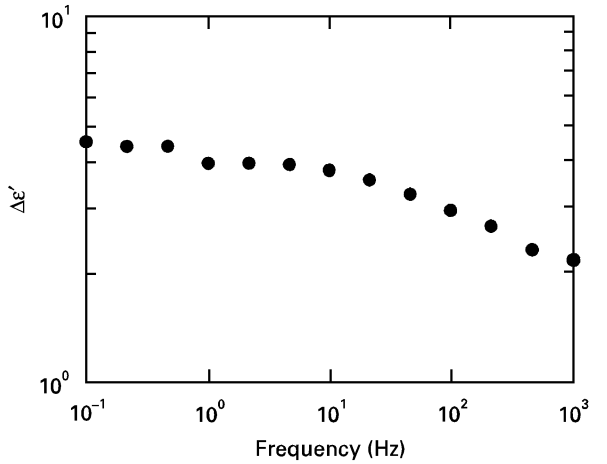

Figure 11 The permittivity of the same sample as in Fig. 10, with the fitted low-frequency dispersion subtracted.

calculations using a b.c.c. and a f.c.c. lattice is remarkable, since they cannot be resolved in Fig. 9a. It thus seems as if the exact geometry is of small importance, with the exception of whether the grains are in contact or not. However, for the high-frequency relaxation, we see that the amplitude differs widely between the different models. Apparently, the exact geometry is of substantial importance for the strength of this relaxation. A random arrangement of the solid particles may yield an even larger relaxation, and also give a distinct relaxation in the model material without interface conduction. Maybe the smoothness of the solid particles also influence the strength of this relaxation.

We note that the predictions of the conductivity using a s.c. lattice has a strange feature; at roughly 100 kHz, it decreases somewhat with increasing frequency. We attribute this to the non-ideality of the calculations; we have only performed the calculations up to the second order in the Fourier expansion of the electric field. Higher-order calculations may thus remove this artefact. For the b.c.c. and f.c.c. lattices, where the solid particles do not touch for this particular value of porosity, this artefact is considerably less pronounced.

It would be tempting to use a model where the solid grains vary in size and are arranged randomly instead of on a regular lattice. Since such calculations are much more complicated, we leave that for future work.

One may ask whether the two relaxations obtained using these models are the only relaxations that occur. We know, for example, that bulk water has a relaxation at roughly 20 GHz at room temperature [44] but, if we restrict ourselves to frequencies where the dispersion of the constituent materials may be considered negligible, do we then obtain more relaxations?

In Fig. 10, we show the dielectric spectrum of a polypropylene sample impregnated with MBT–DBT containing picrates. The reason for showing data for polypropylene is its low dispersion, whereas measurements on sandstone samples in vacuum showed some dispersion. We also show a computer fit to Equation 1 for the low-frequency relaxation. The agreement between the fit and the measured values is good. In Fig. 11, we have plotted the measured ε′, minus the prediction of the above-mentioned fit to

Equation 1. There seems to be only one relaxation left (the Maxwell–Wagner relaxation), and the value of this $\Delta\varepsilon'$ is fairly constant at low frequencies, down to about 0.1 Hz. Below this frequency, the double-layer relaxation is so dominant that it is not possible to extract data with any precision when the effect of the double-layer relaxation is subtracted.

For low frequencies, and high fluid conductivities, we have shown [4] that there appears to be another dielectric relaxation, which we attributed to electrode effects. However, except for the electrode effects, there thus appear only two relaxations when the dispersion of the constituents is negligible.

5.5. Low-frequency relaxation: dependence on porosity and grain size distribution

As discussed above, we have previously found [4] that a fit of the low-frequency relaxation to Equation 1 yields a dependence of the fluid conductivity for A that is comparatively weak, whereas the corresponding dependence for the relaxation time, τ, is stronger. The scattering of the data was too great to draw any definite conclusions on the exact dependence, but the data seemed to follow power laws, with τ and A varying roughly as

$$\tau = \tau_0 \sigma_{\text{liquid}}^{-0.5} \qquad A = A_0 \sigma_{\text{liquid}}^{0.25} \tag{26}$$

Using the same technique as in our previous paper [4], we have calculated A and τ for various values of the fluid conductivity for all our samples. In Figs. 12 and 13, we show the dependences on fluid conductivity of τ and A, respectively, for another sample than in our previous paper (sample S3E having 44% porosity). Also here, data seem to follow roughly the dependence of Equation 26, and similar dependences have also been found for other samples (still showing considerable scatter). We have fitted the obtained dependences to Equation 26, in order to obtain values of A_0 and τ_0 for all our samples. The dependences of τ_0 and A_0 on porosity are shown in Figs. 14 and 15, respectively. The different grain size distributions have different symbols in these plots. There is considerable scatter, and no clear dependence on porosity for τ_0 can be discerned. There appears to be a dependence on grain size distribution, however, with the widest distribution having the highest values of τ_0. Note that the average value of a^2 increases with increasing standard deviation for a log-normal distribution [45], which would imply (following the theory for dilute suspensions of spheres) that the value of τ would increase as the grain size distribution widens. A_0 appears to increase weakly with increasing porosity; it also appears to increase with increasing width of the grain size distribution. We can also check whether the approximate relation in Equation 6, that we found earlier [7] to be roughly valid in the range where $\varepsilon' \propto \omega^{-1.5}$, also applies to A_0. Hence, we plot A_0 as a function of $1/\Lambda F$. Such a comparison is shown in Fig. 16, with a computer fit to a proportionality. The results indicate that Equation 6 may hold, but the large scatter of points prevents a firm conclusion. It should be stressed that there are several sources of

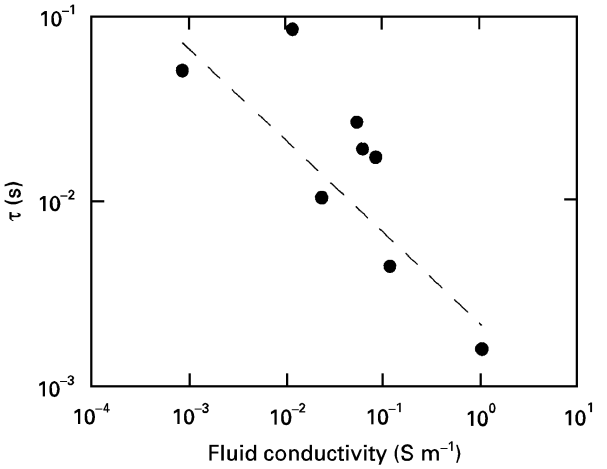

Figure 12 The variation in τ with water conductivity for an impregnated artificial sandstone sample having 44% porosity (sample S3E). (– – –), a computer fit to the relation $\tau = \tau_0 \sigma_{\text{liquid}}^{-0.5}$.

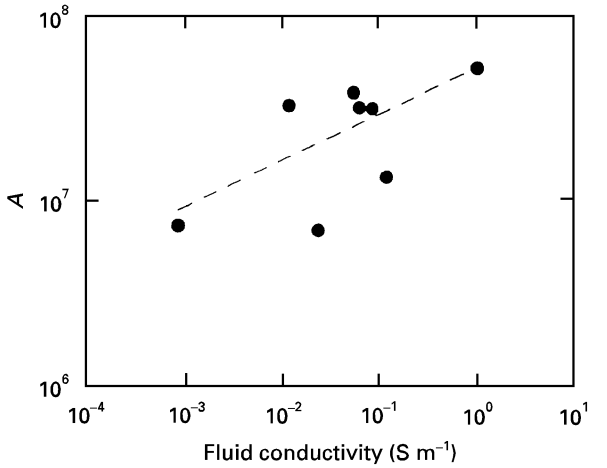

Figure 13 The variation in A with water conductivity for the same sample as in Fig. 12. (– – –) a computer fit to the relation $A = A_0 \sigma_{\text{liquid}}^{0.25}$.

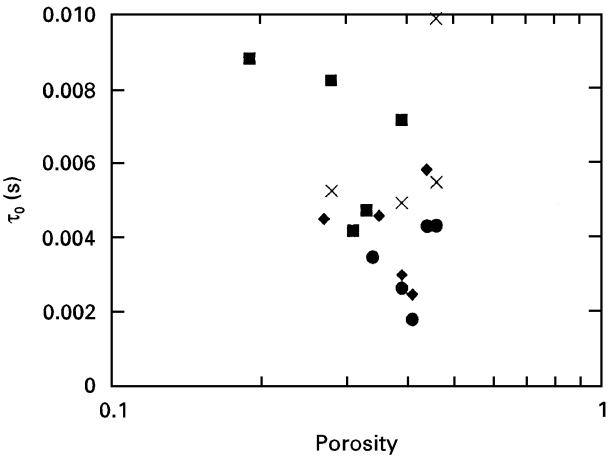

Figure 14 The porosity dependence of τ_0 for the artificial sandstone samples. (●), S1 series; (×), S2 series; (◆), S3 series; (■), S4 series.

error; firstly the measurements of the electrical conductivity and the calculations of the formation factor as well as the measurements of the fluid permeability (needed to obtain Λ), secondly the measurements of

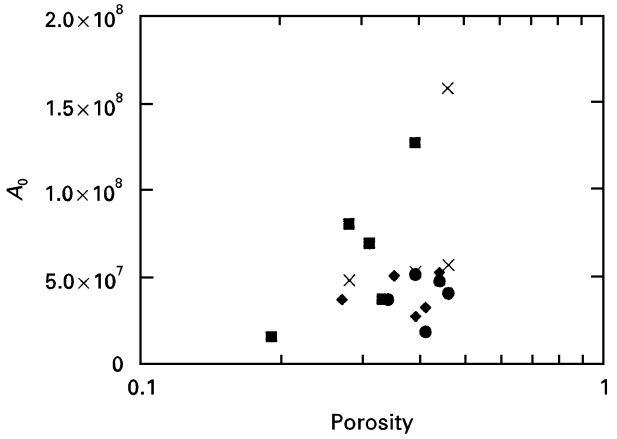

Figure 15 The porosity dependence of A_0 for the artificial sandstone samples. (●), S1 series; (×), S2 series; (◆), S3 series; (■), S4 series.

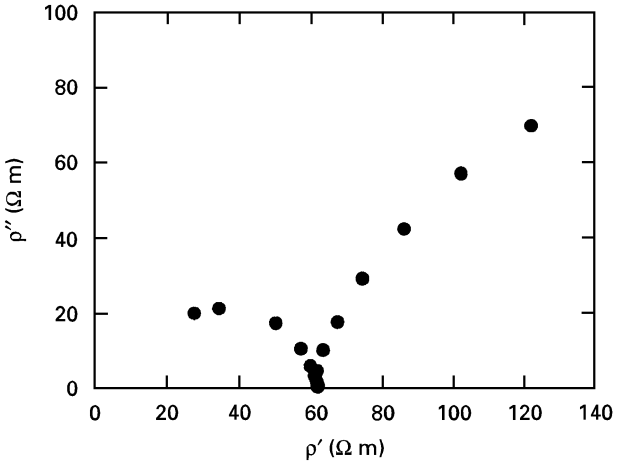

Figure 17 ρ″ as a function of ρ′ for a brine-impregnated sandstone sample. The fluid conductivity was 86 mS m^{-1}, and the sample porosity was 39% (sample S2B).

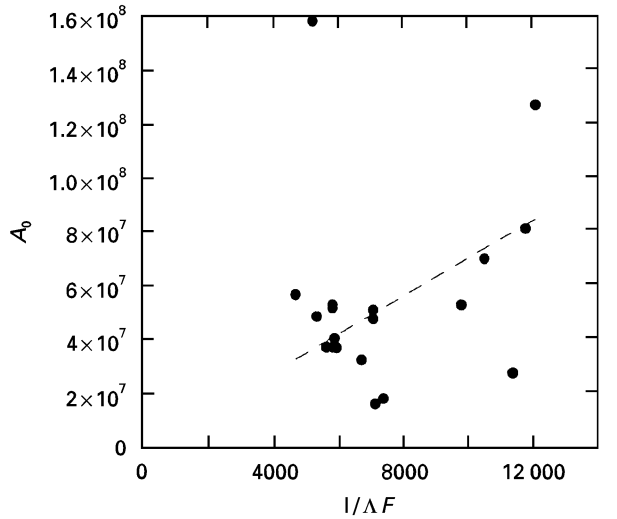

Figure 16 A_0 as a function of $1/\Lambda F$. (– – –), a computer fit to a proportionality.

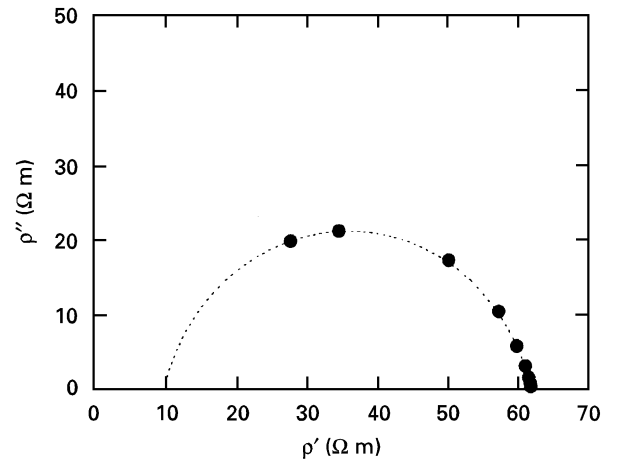

Figure 18 The high-frequency arc of Fig. 17. (-----), a computer fit to a semicircle with the centre on the ρ′ axis.

the permittivity may have errors, thirdly Equation 1 may not be exactly correct in each case, and fourthly Equation 26 may be an approximation to the real dependence. We also assume that c in Equation 6 does not vary among the samples. Still, the agreement is not unreasonable.

5.6. Impregnated samples: Argand diagrams

In Fig. 17, we show measured dielectric data for a typical brine-impregnated artificial sandstone (sample S2B; porosity, 39%; fluid conductivity, 86 mS m^{-1}). The data are displayed in an Argand diagram, i.e., the imaginary part of the resistivity, ρ″, is displayed as a function of the real part of the resistivity, ρ′.

We obtain two arcs in the diagram. None of the arcs is obtained in its entirety, but some characteristics should be noted. It appears as if the low-frequency arc (at high values of ρ′) does not intercept the ρ′ axis at a right angle in its low-ρ′ end, whereas the high-frequency arc appears to intercept the ρ′ axis roughly at a right angle. From this, one could surmise that the high-frequency arc is almost a semicircle (as would be obtained from an equivalent circuit consisting of an ideal capacitor in series with an ideal resistor).

As is shown in Fig. 18, the high-frequency arc can be fitted very well to a semicircle. However, the semicircle obtained from the fit has a high-frequency intercept with the ρ′ axis different from zero value. Similar non-zero intercepts have been obtained from other measurements on brine-impregnated porous solids [46, 47] as well as for water-containing cement [48]. Since the high-frequency part is missing (owing to the frequency limitations of the measurement equipment), the accuracy of the fit in that part of the diagram is highly questionable.

We thus have the possibility that the approximation to a semicircle (with the centre on the ρ′ axis) is invalid. If there is a dielectric relaxation within the frequency range of the arc, there should be deviations from such a semicircle. As we have shown above, there is a relaxation, the Maxwell–Wagner relaxation, which occurs in the pertinent frequency range. Still, if the relaxation occurs close to the frequencies where ρ″ has its maximum, it can be argued that the angles

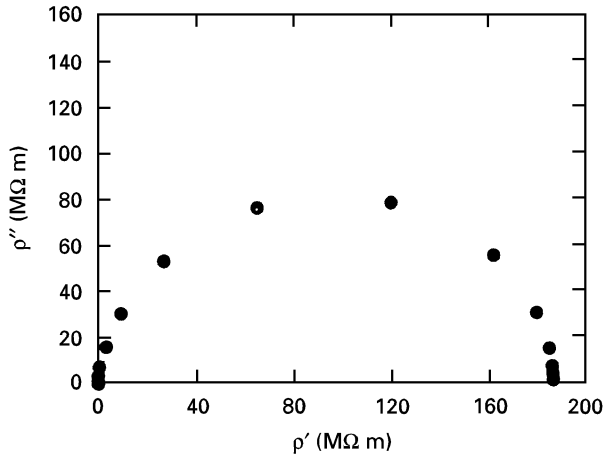

Figure 19 ρ″ as a function of ρ′ for an MBT–DBT-impregnated polypropylene sample. The liquid conductivity was 53 nS m^{-1}, and the sample porosity was 25%.

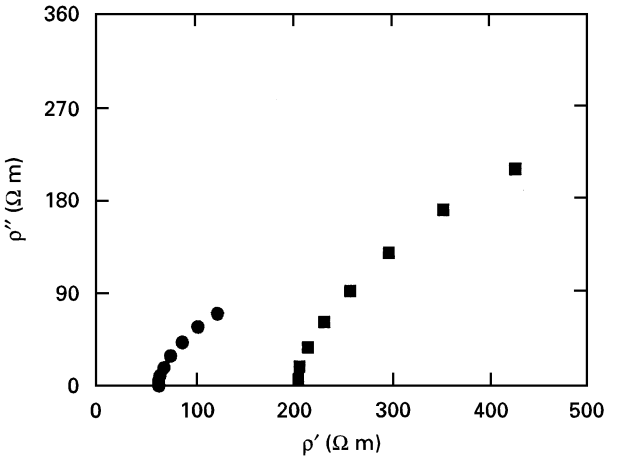

Figure 20 The low-frequency arc of Fig. 17 (●), together with the low-frequency arc of the same sample, impregnated with a liquid having the conductivity 0.0235 Sm^{-1} (■).

between the arc and the ρ′ axis can indeed be 90°, since both ε′ and $\sigma_{a.c.}$ may be almost independent of frequency far from the relaxation frequency. As noted above, we have performed measurements on porous samples consisting of sintered polypropylene beads, impregnated with a MBT–DBT liquid containing ions. An Argand plot from such a measurement is shown in Fig. 19. Here, we obtain the whole high-frequency arc, and it is clearly seen that the results deviate from an ideal *RC* circuit (for which the maximum value of ρ″ is equal to half the maximum value of ρ′). Still, the intercepts with the ρ′ axis are almost at right angles. For artificial sandstones, impregnated with low-conductivity brine solutions, the deviations from an *RC* arc are even smaller. (Data from sandstone samples impregnated with MBT–DBT suffer from the dielectric dispersion of the sand grains, which is not negligible at the frequencies where the arc appears. For such samples, the low-frequency intercept of the arc with the ρ′ axis does not appear to be at a right angle. Polypropylene has much less dispersion than sand.) It should be mentioned that the shapes of the high-frequency arcs are similar for all sandstone samples when impregnated with the same liquid. In particular, when the data are fitted to a semicircle, the ratios, ρ_{hf}/ρ_{mf}, of the values at the two intercepts with the ρ′ axis (see Fig. 18) appear to be roughly the same for all samples, when the same impregnation liquid is used. The ratio is dependent on the conductivity of the pore fluid, however. It accordingly appears as if a finite value of ρ_{hf}, obtained from a fit of the data to a semicircle, cannot be explained as an artefact of the measurement apparatus, as a high-frequency offset resistance due to the apparatus could hardly be proportional to the intermediate-frequency resistance of the sample used.

The low-frequency arc is shown in Fig. 20. We have data only for a part of the arc, and we cannot say how the low-frequency part of this arc would appear. Still, we note that the high-frequency part of the arc does not appear to intercept with the ρ′ axis at a right angle. When increasing the conductivity of the liquid (but using the same sample), the angle appears to increase,

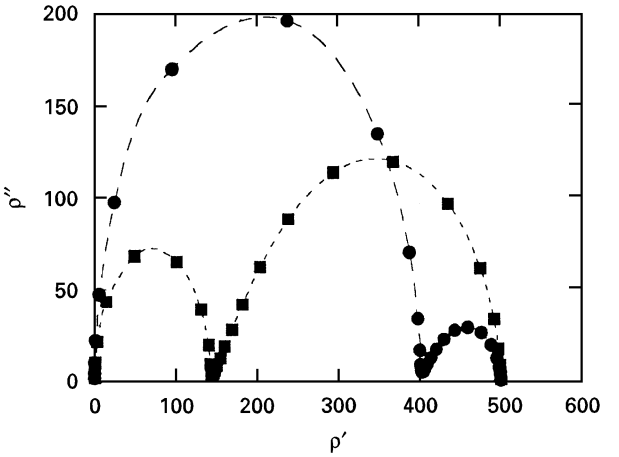

Figure 21 The Argand diagram of a simulated sample, having a dielectric spectrum according to Equation 1. ε_∞ was 80, σ_0 was 2 mS m^{-1}, τ was 1/6π and *A* was 3×10^6 (●) and 3×10^7 (■).

as is also shown in Fig. 20. In fact, Equation 1 yields a similar behaviour. In Fig. 21, we show the Argand diagram for dielectric spectras, obeying Equation 1. We let ε_∞ be 80, σ_0 be 2 mS m^{-1}, τ be 1/6π s and *A* be 3×10^6 and 3×10^7, respectively. The full low-frequency arc is pear shaped, having a low-frequency intercept with the ρ′ axis at a right angle, whereas the high-frequency intercept is at a smaller angle than 90°. We also note that this angle increases as the amplitude *A* increases; in this example, the lower amplitude yields an angle of approximately 33°, whereas the higher amplitude yields an angle of approximately 46°.

For low frequencies, and high values of the liquid conductivity, a third relaxation appears, which we have attributed to electrode effects [4]. The low-frequency Argand diagram for such a sample, impregnated with a brine solution having a conductivity of 0.34 S m^{-1} is shown in Fig. 22a. It appears as if we obtain two arcs, that almost coincide. In Fig. 22b, we show $d(\ln \varepsilon')/d(\ln f)$ as a function of frequency for the same sample. Note that there appears to be a cross-over at roughly 1 kHz, from a low-frequency region, showing an almost constant value, to an intermediate-frequency region, with a much more distinct

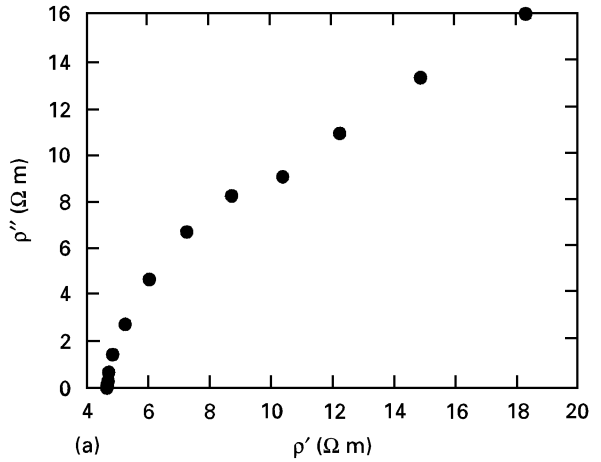

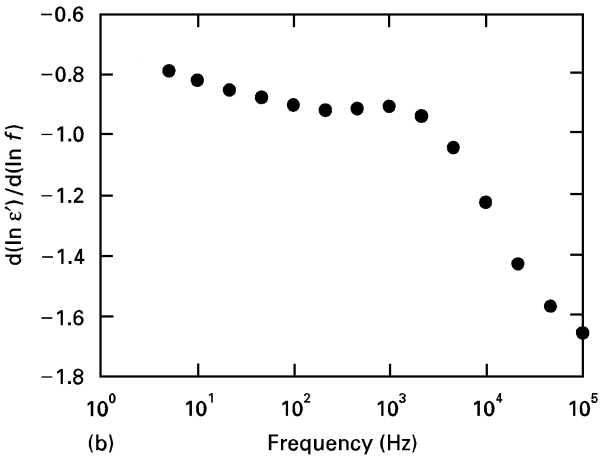

Figure 22 Data for a sample (S2B; porosity, 39%) impregnated with salty water having 0.34 S m^{-1} conductivity. (a) The low-frequency arc of the Argand plot. (b) $d(\ln \varepsilon')/d(\ln f)$ as a function of frequency.

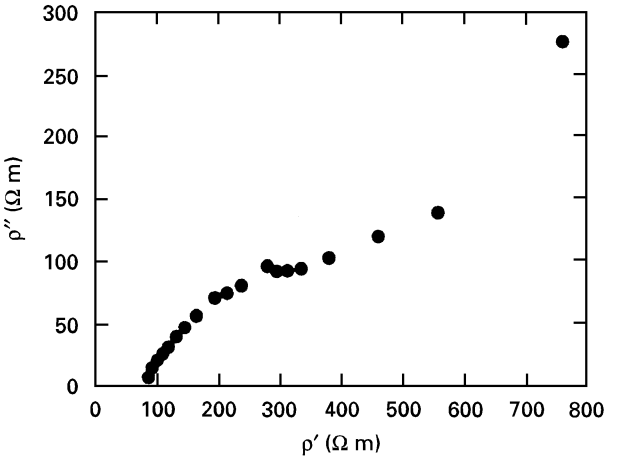

Figure 23 Argand plot for sample S2B (porosity, 39%) impregnated with salty water having a conductivity of 0.13 S m^{-1}. The data were measured between 1 mHz and 1 kHz.

frequency dependence. We have previously [4] interpreted such behaviour as a transition from the dominance of electrode effects at low frequencies to the dominance of the effects of the double layer in the bulk sample at higher frequencies. The arcs appear similar for other samples (although the region where the lowest-frequency electrode arc becomes dominant can vary among the samples and with fluid conductivity). We have tried to fit a semicircle to the arc that dominates at the lowest frequencies; we found that it intercepts with the ρ′ axis at 50–55°. Note that an arc intercepting the ρ′ axis at the angle 45° is obtained from a Randles circuit, which is used to model electrode impedance [49].

We also report results for lower frequencies, down to 1 mHz. In Fig. 23 we show an Argand plot for a sample, measured between 1 mHz and 1 kHz. The impregnation liquid had the conductivity 0.13 S m^{-1}, and almost the entire curve should be dominated by the electrode effects (the only exceptions can be a few points at the low-ρ′ end). We note that the data clearly display an arc, and not a straight line. At the lowest frequencies (high-ρ′ part), we obtain an increase in ρ″; this may be due to a blocking capacitance of the electrodes.

5.7. Suggested equivalent circuit

Our results suggest an equivalent circuit for the system as in Fig. 24. Here, the "double-layer relaxation"

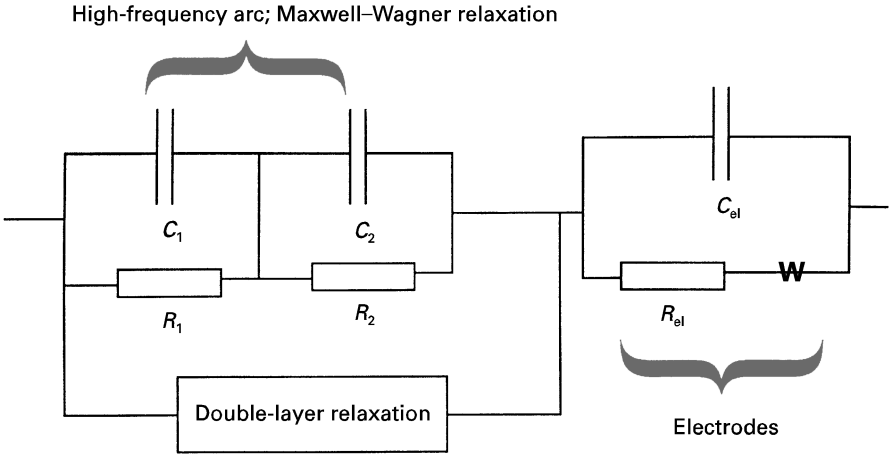

Figure 24 Suggested equivalent circuit for liquid-impregnated porous solids, where the dispersions of the constituent materials are negligible (the capacitors may be frequency dependent).

component is assumed to be described by Equation 1 or by a similar dependence. The W element describes a Warburg impedance [49]. As an initial approach, R_1, R_2, C_1 and C_2 may be assumed to be frequency independent but, in a more general approach, C_1 or C_2 could be assumed to be frequency dependent, for example, constant-phase elements (varying as $C_0(i\omega)^{-\alpha}$). The need for *two RC* circuits arises from the Maxwell–Wagner relaxation at high frequencies. The interface layer should form a percolating path throughout the porous material and we accordingly let it be in parallel to the *RC* circuits. However, the model calculations have shown that the amplitude of the Maxwell–Wagner relaxation is dependent on the strength of the double-layer relaxation. It may thus be physically more correct to split the double-layer relaxation into two parts, each in parallel to either of the *RC* circuits, to render the Maxwell–Wagner relaxation dependent on the amplitude of the double-layer relaxation.

The Randles circuit used for describing electrode effects may also be more complicated than shown in Fig. 24. For example, the capacitor C_{el} may also be a constant-angle element.

5.8. High-frequency permittivity: porosity dependence

For the high-frequency measurements, we have noticed a slight increase in capacitance with increasing frequency for frequencies above 4 MHz. We interpret this as an instrumentation artefact, as the manufacturer explicitly declares that the accuracy of the equipment is less good at the highest frequencies. Normally, we found that the frequency dependence around 4 MHz is rather weak, and we thus use the value of ε' at 4 MHz as a "high-frequency" value. In Fig. 25, we show the value of ε' at 4 MHz for a typical sample (sample S1E, having 46% porosity) as a function of the fluid conductivity. For low values of the fluid conductivity, ε' appears to be constant, whereas it appears to decrease with increasing fluid conductivity for conductivities larger than 50 mS m^{-1}. This is probably an effect of the Maxwell–Wagner relaxation, which should move upwards in frequency as the fluid conductivity is raised. The values of ε' at 4 MHz at fluid conductivities below 50 mS m^{-1} accordingly appear to be a good measure of the high-frequency permittivity of the brine-sand system. (Poley *et al.* [50] found that the permittivity is independent of salinity for sufficiently low salinities and sufficiently high frequencies. The value of 50 mS m^{-1} for a frequency of 4 MHz is consistent with their data if we assume that the relaxation frequency is proportional to the liquid conductivity.)

In Figs. 26 and 27, we show the obtained high-frequency permittivity as a function of porosity. We also include the porosity dependences, predicted by the mixing theories discussed previously (Equations 10–16). In the theoretical calculations, we assumed ε_{sand} to be 4.3. We also used Equation 10 with β as an adjustable parameter to obtain the optimal fit; the optimal value of β was found to be 0.68.

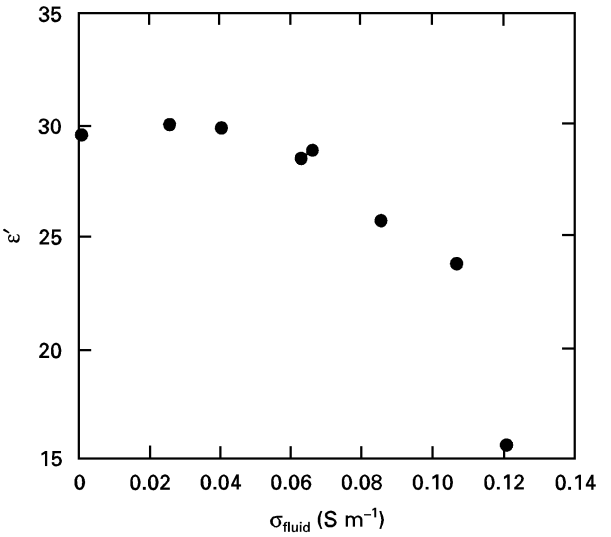

Figure 25 The permittivity at 4 MHz for a brine-impregnated artificial sandstone sample having 46% porosity (sample S1E) as a function of the fluid conductivity.

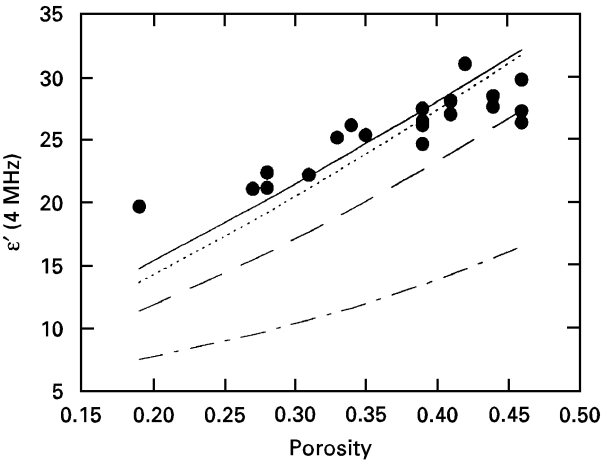

Figure 26 The permittivity at 4 MHz for low fluid conductivity of brine-impregnated artificial sandstones as a function of porosity. (——), calculation according to the Maxwell Garnett expression (Equation 15); (-----), calculation according to Equation (10), having β as an adjustable parameter; (– –), calculation according to the CRIM equation (Equation 11); (– – –), calculation according to the Lichtenecker equation (Equation 13).

The best agreements between model predictions and experiments were obtained with the Maxwell Garnett expression (Equation 15) and with Equation 10 using β as an adjustable parameter. The other expressions show deviations from the experimental data, particularly at low values of the porosity. The Lichtenecker formula has the strongest deviation from the experimental results of all the formulae used; it does not even appear to approach the experimental data at higher values of porosity.

Note, however, that for the highest values of the porosity the Maxwell Garnett expression and Equation 10 using β as an adjustable parameter start to deviate from the behaviour of the experimental data, while the CRIM and the Bruggeman–Hanai expressions here have slightly better agreement with experiments.

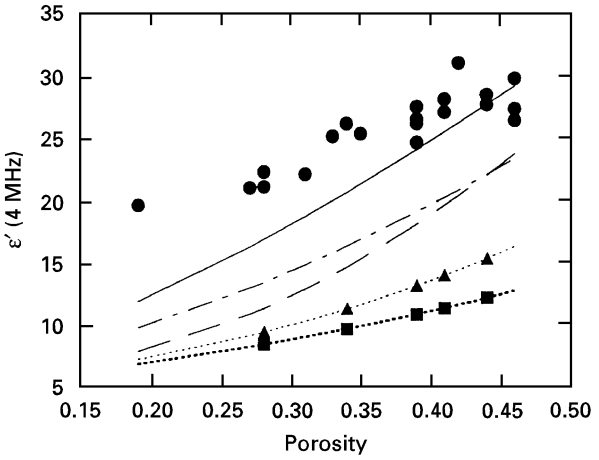

Figure 27 The same data as in Fig. 26, together with calculations according to the Bruggeman–Hanai expression (Equation 16) (——), to the expression of Looyenga and of Landau and Lifshitz (Equation 12) (– – –), to the symmetric Bruggeman expression (Equation 14) (– –) and to the Maxwell Garnett expression (---▲---) and the Bruggeman–Hanai expression (---■---), treating water as the guest phase.

Finally, we have also examined the effect of letting the water function as the guest phase in the asymmetric models. As is shown in Fig. 27, those results deviate considerably from the experimental data.

6. Conclusions

For a liquid-impregnated porous solid, where the dielectric dispersions both of the bulk liquid and of the bulk solid are negligible, we find that two dielectric relaxations arise, as well as a third process which we attribute to electrode effects.

Using model calculations, we found that the surface conductivity and the low-frequency permittivity found in artificially made sandstone samples are related in a consistent way.

The surface conductivity was found to cause a polarization of Maxwell–Wagner type at high frequencies. This relaxation would probably occur in real samples even without interface conduction, but it would then be smaller in amplitude. In our models, the high-frequency relaxation almost disappeared when no interface conductivity was used. The strength of the relaxation has a pronounced dependence of the geometry of the porous solid, however.

In the experiments we could only see the lower part of this polarization process. Nevertheless, the relaxation frequency predicted by the DEM theory is of the right order of magnitude, while the GCM predicts a much higher relaxation frequency. At low frequencies, we observe an increase in the values of ε'. We have previously shown [2, 4] that this increase emanates from the " bulk sample ". To model this effect, we assumed that the frequency behaviour of the interface varies according to Equation 1. Here, we found that the low-frequency conductivity, σ_0, of the interface layer is negligible, compared with the amplitude of the low-frequency relaxation, at least for low values of σ_f. We also noted that the exact geometry (for a given porosity) seems to be of little importance for this relaxation.

In a so-called Argand plot, the dielectric spectrum gives rise to two arcs. The high-frequency arc deviates somewhat from a semicircle, something which we attribute to the Maxwell–Wagner relaxation which occurs in the frequency range of the high-frequency arc. The low-frequency arc intercepts at its high-frequency end with the ρ' axis at an angle smaller than 90°. The angle apparently increases with increasing conductivity of the fluid. The full arc would probably appear to be pear shaped; however, at still lower frequencies, electrode effects become dominant. Such effects appear roughly as the response of a Randles circuit. We also tested several mixing rules. The scatter of the data for unimpregnated samples made evaluation of the different formulae difficult. However, it should be noted that, for asymmetric formulae, better agreement was obtained when the sand grains were used as a host material than when they were used as a guest material. For impregnated samples, we found that the Maxwell Garnett formula (Equation 15), having the sand grains as the guest material, yielded the results that showed the best agreement with experimental data.

Acknowledgements

This work was in part supported by the Swedish Natural Science Research Council. We wish to thank Bengt Åhlén for providing the artificial sandstone samples, Per Albihn at the Swedish Institute for Fibre and Polymer Research for providing the polypropylene, Å. Hammarsten at ABB Capacitors for providing the toluene liquids and J. Bergman and the Royal Institute of Technology for providing the picrates. One of us (B.N.) is grateful for financial support from ABB Corporate Research.

References

1. P. R. CAMP and S. BILOTTA, *J. Appl. Phys.* **66** (1989) 6007.
2. B. NETTELBLAD and G. A. NIKLASSON, *Solid State Commun.* **90** (1994) 201.
3. B. NETTELBLAD, B. ÅHLÉN, G. A. NIKLASSON and R. M. HOLT, *J. Phys. D: Appl. Phys.* **28** (1995) 2037.
4. B. NETTELBLAD and G. A. NIKLASSON, *J. Phys.: Condens. Matter* **7** (1995) L619.
5. B. NETTELBLAD, *J. Appl. Phys.* **79** (1996) 7106.
6. B. NETTELBLAD and G. A. NIKLASSON, *J. Phys.: Condens. Matter* **8** (1996) 2781.
7. *Idem., J. Phys.: Condens. Matter* **8** (1996) 7049.
8. D. A. LOCKNER and J. D. BYERLEE, *J. Geophys. Res.* **90** (1985) 7837.
9. C. RUFFET, Y. GUEGUEN and M. DAROT, *Terra Nova* **3** (1991) 265.
10. W. C. CHEW and P. N. SEN, *J. Chem. Phys.* **77** (1982) 4683.
11. B. NETTELBLAD and G. A. NIKLASSON, *J. Colloid Interface. Sci.* **181** (1996) 165.
12. V. N. SHILOV and Y. B. BORKOVSKAYA, *Colloid J.* (*Engl. Transl.*) **56** (1994) 724.
13. B. NETTELBLAD and B.-E. MELLANDER, *IEEE Trans. Dieletr. Electr. Insul.* **3** (1996) 99.
14. K. W. WAGNER, *Arch. Elektrotech.* **2** (1914) 371.
15. G. BLUM, H. MAIER, F. SAUER and H. P. SCHWAN, *J. Phys. Chem.* **99** (1995) 780.
16. W. I. ARCHER and R. D. ARMSTRONG, in " Electrochemistry, Vol. 7 edited by H. R. Thirsk (Chemical Society, London, 1980) p. 157.

17. D. L. JOHNSON, J. KOPLIK and L. M. SCHWARTZ, *Phys. Rev. Lett.* **57** (1986) 2564.
18. D. L. JOHNSON and P. N. SEN, *Phys. Rev. B* **37** (1988) 3502.
19. P. N. SEN, P. A. GOODE and A. SIBBIT, *J. Appl. Phys.* **63** (1988) 4832.
20. P. N. SEN and P. A. GOODE, *Geophysics* **57** (1992) 89.
21. L. M. SCHWARTZ, P. N. SEN and D. L. JOHNSON, *Phys. Rev. B* **40** (1989) 2450.
22. R. LANDAUER, in "Proceedings of the Conference on Electrical, Transport and Optical Properties of Inhomogeneous Media" (American Institute of Physics, New York, 1977) p. 2.
23. G. BÁNHEGYI, *Colloid Polym. Sci.* **264** (1986) 1030.
24. B. R. DE, *Log Analyst* **27** (1986) 63.
25. H. LOOYENGA, *Physica* **31** (1965) 401.
26. L. D. LANDAU and E. M. LIFSHITZ, "Electrodynamics of continuous media" (Pergamon, Oxford, 1960).
27. K. LICHTENECKER, *Phys. Z.* **27** (1926) 115.
28. D. A. G. BRUGGEMAN, *Ann. Phys., Lpz.* **24** (1935) 636.
29. J. C. MAXWELL GARNETT, *Phil. Trans. R. Soc. A* **203** (1904) 385.
30. T. HANAI, *Kolloid Z.* **171** (1960) 23.
31. C. BONED and J. PEYRELASSE, *Colloid Polym. Sci.* **261** (1983) 600.
32. J. N. ROBERTS and L. M. SCHWARTZ, *Phys. Rev. B* **31** (1985) 5990.
33. L. M. SCHWARTZ and S. KIMMINAU, *Geophysics* **52** (1987) 1402.
34. L. C. SHEN, C. LIU, J. KORRINGA and K. J. DUNN, *J. Appl. Phys.* **67** (1990) 7071.
35. B. NETTELBLAD and G. A. NIKLASSON, in "Proceedings of the conference on Dielectric and Related Phenomena", 1994 (Cracow Institute of Technology, Zakopane, 1994) p. 95.
36. R. C. WEST (Ed) "CRC handbook of chemistry and physics" (Chemical Rubber Company, Cleveland, OH, 1973) p. E48.
37. E. H. B. DeLACEY and L. R. WHITE, *J. Chem. Soc., Faraday Trans. II* **77** (1981) 2007.
38. E. FJAER, R. M. HOLT, J. S. RATHORE and B. ÅHLÉN, *Geophys. J.* **107** (1991) 687.
39. B. ÅHLÉN, Licentiate Thesis, Chalmers University of Technology (1993).
40. U. GÄFVERT and B. NETTELBLAD, in "Proceedings of the Nordic Insulation Symposium NORD-IS '90", (Danmarks tekniske højskole, Lyngby, Denmark, 1990) Paper 7.1.
41. W. E. KENYON, *J. Appl. Phys.* **55** (1984) 3153.
42. I. HOLWECH and B. NØST, *Phys. Rev. B* **39** (1989) 12845.
43. A. L. ENDRES and R. J. KNIGHT, *J. Colloid Interface Sci.* **157** (1993) 418.
44. U. KAATZE, *J. Chem. Engng Data* **34** (1989) 371.
45. J. AITCHISON and J. A. C. BROWN, "The lognormal distribution" (Cambridge University Press, Cambridge, Cambs., 1957).
46. R. J. KNIGHT and A. NUR, *Geophysics* **52** (1987) 644.
47. A. A. GARROUCH and M. M. SHARMA, *ibid.* **59** (1994) 909.
48. B. J. CHRISTENSEN, R. T. COVERDALE, R. A. OLSON, S. J. FORD, E. J. GARBOCZI, H. M. JENNINGS and T. O. MASON, *J. Amer. Ceram. Soc.* **77** (1994) 2789.
49. I. D. RAISTRICK, J. R. MACDONALD, D. R. FRANCESHETTI, in "Impedance spectroscopy", edited by J. R. Macdonald (Wiley, New York, 1987) p. 27.
50. J. P. POLEY, J. J. NOOTEBOOM and P. J. de WAAL, *Log Analyst* **19** (1978) 8.

Received 8 May 1996
and accepted 20 January 1997